Published in final edited form as:

Small. 2018 January ; 14(4): . doi:10.1002/smll.201702479.

Miniaturized, Battery-Free Optofluidic Systems with Potential for Wireless Pharmacology and Optogenetics

Kyung Nim Noh,
Department of Electrical and Computer Engineering, University of Illinois at Urbana-Champaign, Urbana, IL 61801, USA

Prof. Sung Il Park,
Department of Electrical and Computer Engineering, Texas A&M University, College Station, TX 77843, USA

Center for Remote Health Science Technologies, Texas A&M University, College Station, TX 77843, USA

Raza Qazi,
Department of Electrical, Computer, and Energy Engineering, University of Colorado Boulder, Boulder, CO 80309, USA

Zhanan Zou,
Department of Mechanical Engineering, University of Colorado Boulder, Boulder, CO 80309, USA

Dr. Aaron D. Mickle,
Department of Anesthesiology, Washington University Pain Center, Washington University School of Medicine, St. Louis, MO 63130, USA

Jose G. Grajales-Reyes,
Department of Anesthesiology, Washington University Pain Center, Washington University School of Medicine, St. Louis, MO 63130, USA

Kyung-In Jang,
Department of Robotics Engineering, Daegu Gyeongbuk Institute of Science and Technology (DGIST), Daegu 42988, Republic of Korea

Prof. Robert W. Gereau IV,
Department of Anesthesiology, Washington University Pain Center, Washington University School of Medicine, St. Louis, MO 63130, USA

Department of Neuroscience, Washington University Pain Center, Washington University School of Medicine, St. Louis, MO 63130, USA

Prof. Jianliang Xiao,

Correspondence to: John A. Rogers; Jae-Woong Jeong.

Supporting Information

Supporting Information is available from the Wiley Online Library or from the author.

Conflict of Interest

The authors declare no conflict of interest.

The ORCID identification number(s) for the author(s) of this article can be found under https://doi.org/10.1002/smll.201702479.

Department of Mechanical Engineering, University of Colorado Boulder, Boulder, CO 80309, USA

Prof. John A. Rogers, and
Department of Materials Science and Engineering, Biomedical Engineering, Neurological Surgery, Chemistry, Mechanical Engineering, Electrical and Computer Science, Northwestern University, Evanston, IL 60208, USA

Center for Bio-Integrated Electronics, Simpson Querrey Institute for BioNanotechnology, Northwestern University, Evanston, IL 60208, USA

Prof. Jae-Woong Jeong
Department of Electrical, Computer, and Energy Engineering, University of Colorado Boulder, Boulder, CO 80309, USASchool of Electrical Engineering Korea Advanced Institute of, Science and Technology (KAIST), Daejeon 34141, Republic of Korea

Abstract

Combination of optogenetics and pharmacology represents a unique approach to dissect neural circuitry with high specificity and versatility. However, conventional tools available to perform these experiments, such as optical fibers and metal cannula, are limited due to their tethered operation and lack of biomechanical compatibility. To address these issues, a miniaturized, battery-free, soft optofluidic system that can provide wireless drug delivery and optical stimulation for spatiotemporal control of the targeted neural circuit in freely behaving animals is reported. The device integrates microscale inorganic light-emitting diodes and microfluidic drug delivery systems with a tiny stretchable multichannel radiofrequency antenna, which not only eliminates the need for bulky batteries but also offers fully wireless, independent control of light and fluid delivery. This design enables a miniature (125 mm^3), lightweight (220 mg), soft, and flexible platform, thus facilitating seamless implantation and operation in the body without causing disturbance of naturalistic behavior. The proof-of-principle experiments and analytical studies validate the feasibility and reliability of the fully implantable optofluidic systems for use in freely moving animals, demonstrating its potential for wireless in vivo pharmacology and optogenetics.

Keywords

battery-free; fully implantable; neural; optofluidic; wireless

We present materials and soft electronics design strategies for fully implantable, battery-free, wireless optofluidic systems that are highly versatile and can be used for in vivo optogenetics and pharmacology experiments in freely behaving animals. Our design combines a multimodal neural probe consisting of microscale inorganic light-emitting diodes (μ-ILEDs) and microfluidic drug delivery systems with a stretchable radiofrequency (RF) energy-scavenging circuit into an ultracompact, lightweight, soft platform. Due to its small size and biocompatible features, our device can not only be implanted in the brain but could also potentially be adapted to experiments in the peripheral nervous system. The current design obviates a large battery pack and associated power management circuits, enabling a dramatic reduction in volume (from 1575 to 125 mm^3) and weight (from 1860 to 220 mg) when compared to the previously reported wireless optofluidic systems.[1,2] This

technology has immense potential to open up new opportunities for complex neuroscience experiments as well as clinical applications by allowing seamless and untethered integration into various space-critical locations in the body (e.g., brain, spinal cord, peripheral nerves, etc.), thereby allowing naturalistic behavior during in vivo operation.

Optogenetics[3] and pharmacology[4] are important biological techniques that have shown enormous promise for dissecting neural circuits,[5] treating neurodegenerative diseases such as Parkinson's and Alzheimer's,[6,7] deciphering decision-making processes[8] as well as many other applications.[9–12] The traditional approaches of using optical fibers for light delivery and metal cannulas for drug infusion are based on rigid materials (E H ≈ 16 GPa for optical fibers with coating and ≈200 GPa for metal cannulas) and a tethered operation. These attributes significantly limit the potential of optogenetics and pharmacology techniques by causing severe neural tissue damage[13,14] and restricting the subject's movements.[15] Recent advances in this field have demonstrated the use of flexible neural implants[1,16–22] and wireless technologies[1,23–26] to enable minimally invasive chronic implantation and untethered neuromodulation, respectively, in freely moving animals. To achieve wireless optogenetics and pharmacology, we recently introduced a head-mounted, infrared (IR) wireless optofluidic device, which offers wireless control of both light and fluid delivery into deep brain tissue via a flexible optofluidic probe.[1] While innovative, these devices require batteries to power the wireless circuit, making them bulky and preventing prolonged continuous operation due to the need for intermittent recharging of batteries. The relatively large size of these head-mounted devices also limits the applications to the brain, where the device can be mounted without severely interfering with rodents normal behavior. Here we expand on this technology and report a new type of ultracompact, soft wireless optofluidic system that surpasses existing technologies in its significantly smaller size with wireless powering capabilities. Advanced features enabled by a tiny stretchable multichannel antenna allow fully wireless, battery-free control of light and fluid delivery and extend its potential applications to not only the brain but also the spinal cord and the peripheral nervous system by permitting full implantation. Theoretical analysis using a phantom model and experimental characterization via successful implantation in a live mouse verify the functional capabilities and biological safety, demonstrating our device's potential for use in freely behaving animals.

Figure 1 shows the design of our fully implantable, battery-free, wireless optofluidic system. The device consists of an array of μ-ILEDs (220 μm × 270 μm × 50 μm; C450TR2227-0214, Cree Inc.), a flexible microfluidic probe, a stretchable two-channel RF wireless energy harvester, and a thermally actuated fluid reservoir, which uses thermal expansion of a layer (a mixture of polydimethylsiloxane (PDMS) and expandable microspheres (Expancel 031 DU 40, AkzoNobel) with a ratio of 2:1) via Joule heating (Figure 1A and Figure S1, Supporting Information). The reservoir (0.5 μL) is composed of cyclic olefin polymer, which has very low water vapor permeability (0.023 g mm m^{-2} d^{-1}) and supports prolonged storage of fluid. A copper membrane (3 μm thick) hermetically seals the outlet of the reservoir to prevent fluid evaporation. The soft, flexible, and stretchable design in a small footprint (RF harvester: 5.8 mm × 9 mm × 1 mm; fluidic reservoir: 5.8 mm × 4.2 mm × 3 mm; probe: 500 μm × 8 mm × 80 μm; total weight: 220 mg) enables minimally invasive, seamless implantation into brain tissue (Figure 1B–D and Figure S2, Supporting

Information). The pliable and elastic device body allows conformal integration onto the curvilinear surface of the brain, while the ultrathin, flexible probe facilitates deep injection into brain tissue with minimal tissue damage.[1] Our optofluidic probe is more than six times thinner and approximately five orders of magnitude more compliant than the conventional metal cannula (80 μm thick, 13–18 N m^{-1} in bending stiffness for the optofluidic probe vs 500 μm thick, >5 MN m^{-1} for the 26-gauge metal cannula; Figure 1D and Figure S2, Supporting Information).[1] Moreover, this PDMS-based probe offers even higher flexibility compared to other types of polymer microfluidic probes[17,27–30] due to its significantly lower elastic modulus (≈1 MPa for PDMS vs 2.2 GPa for parylene C, 2.5 GPa for polyimide, and ≈2.7 GPa for thermally drawn fibers).[21,31] These attributes enable adaptation to the micromotion of neural tissue, making the probe suitable for chronic implantation and minimizing tissue damage and inflammatory responses.

A key to miniaturizing our devices is a tiny stretchable, multichannel ultrahigh-frequency range antenna that integrates multiple serpentine capacitive traces and yields nonoverlapping operation channels. This component not only makes the device smaller and lighter but also enables battery-free wireless control of the μ-ILEDs and the fluid pump for optical and/or pharmacological manipulation of neural circuits. Details of the device design are shown in Figure S3 in the Supporting Information and the Experimental Section. The two-channel stretchable antenna integrates two pairs of serpentine metal traces (channel 1: green and blue traces; channel 2: blue and red traces; Figure 1E), each of which provide a separate channel at a different frequency via capacitive coupling between two distinct traces. It has a tunable nature of operation frequencies where reduction (increase) of spacing between serpentine traces induces more (less) coupling between traces and thereby lowers (increases) the resonant frequency.[32] Collectively, frequency selective energy harvesting yields nonoverlapping channels, enabling the harvester to allow independent or simultaneous control of light and fluid deliveries as shown in Figure 1F–H. A fascinating feature of this approach is that the design is scalable for independent control over many active components. In other words, the number of antenna channels can be increased for more versatile operations of neural devices, as demonstrated in Figures S4 and S5 in the Supporting Information for independent control of four reservoirs using a four-channel harvester. Integrating multiple reservoirs and optical channels opens opportunities to modeling more complex circuit behavior in a minimally invasive manner with no phototoxicity compared to existing optogenetic techniques.[33,34]

Figure 2 shows characteristics of the two-channel wireless optofluidic systems. The experimental setup for device operation is depicted in Figure 2A and Figure S6 in the Supporting Information. The device (dotted box in Figure 2A) harvests energy by capturing RF electromagnetic waves sent from a remotely located wireless power transmitter, consisting of a signal generator and an RF power amplifier ($Gain_{1dB}$ = 50 dB) and delivers rectified and multiplied voltages to its active components (i.e., a heater for fluid delivery in channel 1; μ-ILEDs for optical stimulation in channel 2). The wireless harvester is designed to have peak power transmission efficiencies at 1.8 GHz (channel 1) and 2.9 GHz (channel 2) for independent and selective control of two separate channels (Figure 2B). The sufficient separation of the resonant frequencies of the two channels effectively suppresses crosscoupling of transmitted power, thus preventing undesired activation of a nontargeted

channel (see the Supporting Information). For optogenetic applications involving light sensitive opsin such as Channelrhodopsin, optical power density higher than ≈1 mW mm^{-2} is necessary at a wavelength of ≈450 nm.[16] The characterization in Figure 2C shows that operation of the device with the transmitted RF power of 0.2 W from 10 cm away achieves sufficient optical power density (≈30 mW mm^{-2}), which is more than enough for typical optogenetic experiments. For complete delivery of fluid stored in the reservoir, the heater temperature should be greater than ≈87 °C for sufficient expansion of the expandable layer in the reservoir.[1] Transient behaviors of the heater temperature with different transmitted powers at channel 1 (Figure 2D) demonstrate that operation with 2 W average transmitted power is adequate to meet this requirement. With the 2 W transmitted power, the heater temperature reaches ≈100 °C and can pump out ≈0.46 μL of fluid from the reservoir in 25 s (Figure 2E–G). If the transmitting antenna is operated from a distance of 10 cm or closer to the optofluidic device, the RF operation power required to activate these devices in animals does not exceed the values suggested by the Federal Communications Commission (FCC) guideline (4 W Equivalent Isotropically Radiated Power, FCC 15.247),[35] confirming biologically safe operation for in vivo experiments.

Understanding the effects of mechanical deformation of the stretchable antenna can provide insights into device design and operation in a physiological environment. Physiological strain that occurs during animals' movement can deform metallic traces of the implanted device so that it induces enhanced or reduced capacitive coupling, thereby shifting the center frequency of operation. Such shifting may prevent proper activation of the device by causing mismatch of the center frequencies between the harvester and the transmitter. Systematic studies with electromechanical simulations on the multichannel stretchable antenna under horizontal, vertical, and diagonal deformations of 20% (assuming the worst-case scenarios in biological tissue) reveal that the antenna features relatively wide bandwidths, making it less sensitive to variations in center frequencies and thereby ensuring reliable activation of the device within tissue in dynamic motion (Figure 3).

Finite element analysis (FEA) of our device (Figure 3,i; Abaqus, Dassault Systemes) reveals that the antenna design with serpentine traces allows stretching over 20% with only ≈1% maximum principal strain in the metal traces (fracture strain of Cu: 20%–40%)[36] for the following scenarios: uniaxial horizontal stretching (Figure 3A), uniaxial vertical stretching (Figure 3B), and biaxial diagonal stretching (Figure 3C). The applied strain causes the spacing between traces in the strain direction to increase while decreasing it more significantly in the orthogonal direction of the strain, thus shifting down the resonant frequencies (Figure 3,ii: Figure 3A, 30 and 100 MHz shifts; Figure 3B, 70 and 70 MHz shifts; Figure 3C, 80 and 80 MHz shifts for channels 1 and 2, respectively). If the transmitter output frequencies are unchanged from the original setting when the antenna is deformed, the resonant frequency shift makes the S_{11} (reflected power at antenna) increase from its original value, therefore degrading the RF power transmission efficiencies. For the fluidic channel (channel 1; blue in Figure 3,ii), an increase in the reflected power can potentially keep the heater temperature from reaching our target temperature of ≈87 °C. When operated with 2 W average transmitted power, the heater temperature at 25 s decreases by 3% (Figure 3A,iii), 3.4% (Figure 3B,iii), and 4.3% (Figure 3C,iii) for 20% horizontal, vertical, and diagonal stretching of the antenna, respectively. Similarly, the total optical output power

density in the μ-ILED probe decreases by 9% (Figure 3A,iv), 3.4% (Figure 3B,iv), and 3.7% (Figure 3C,iv) for 20% horizontal, vertical, and diagonal deformation, respectively, when controlled with 0.2 W transmitted power. While the demonstrated deformation is an extreme condition, which is unlikely in the brain or other nervous system tissues, a ≈5% increase in transmitted power (from 2 to 2.1 W) can ensure proper operation of the thermally actuated pump even with the deformed antenna. Unlike the heater case, decreases in optical output powers in these three scenarios result in power densities that are still sufficiently high for typical optogenetic activation, suggesting robust functionality under extreme deformation. Moreover, the frequency shift does not affect the resonant frequency spacing, maintaining appropriate channel isolation for independent operation of each channel.

Experimental and analytical studies (Figure 4) validate the feasibility and reliability of the fully implanted optofluidic systems for use in freely moving animals. To simulate in vivo operation, the device is implanted in the phantom brain (0.6% agarose gel) of a model rat, which is filled with saline solution to provide similar RF characteristics to biological tissue (Figure S7, Supporting Information). The implanted device is encapsulated with a 2 mm thick PDMS layer, which acts as a buffer to prevent thermal damage of interfacing tissue due to high temperature fluidic actuation (Figure 4A). Measurement using an IR thermal imager and FEA simulation (Abaqus, Dassault Systemes) indicates that this thermal buffer layer effectively dissipates the heat generated from the heater for biothermal compatibility. When the heater temperature increases to ≈100 °C for fluid delivery, the temperature at the tissue interface (PDMS encapsulant surface) of the device reaches only ≈30 °C in an ambient environment at room temperature (Figure 4B and Figure S8, Supporting Information); when integrated onto the brain, the PDMS encapsulant limits the temperature increase on the brain surface to <0.5 °C, thus enabling biologically safe operation (Figure 4C). Previous studies have also shown that fluid stored inside the reservoir remains at a temperature below ≈60 °C during delivery and rapidly cools down to surrounding temperature before reaching the target tissue.[1] The thermal safety of μ-ILEDs operation for in vivo optogenetics has been verified in our previous studies.[16,24,25,37]

It is important for the device to stably harvest transmitted RF energy to support reliable performance in freely moving animals. Omnidirectional electromagnetic radiation patterns for both channels enable robust and uniform activation of the device regardless of its orientation and angle (Figure 4D–F). Figure 4G provides visual evidence of reliable operation in an experimental setup using model rats at various angular orientations. This feature ensures reliable and robust wireless operation for light and fluid delivery regardless of the device orientation with respect to the transmitting antenna. Additionally, preliminary experiments with mice demonstrate the potential of our device for in vivo operation (Figures 4H,I and Figure S9, Supporting Information).

These fully implantable, battery-free, wireless optofluidic systems have enormous potential for use in in vivo optogenetics and pharmacology with possible future applications in optopharmacology. The miniaturized geometry and soft construction of these devices enables their implantation into the brain as well as other biological tissues. Straightforward extension of the number of operation channels via an advanced impedance matching technique can offer opportunities for more versatile implementation of various functions of

neural implants for complex neuroscience research and clinical applications. Such an approach will allow dissection of neural circuits in a dual fashion, using light to modulate neuronal activity via optogenetics, while allowing localized administration of pharmacological agents targeting multitude cellular pathways that mediate neuronal physiology. In addition, due to the device design and integration of μ-ILEDs with a multiple-chamber reservoir, multiple rounds of drug administration can be performed. This feature can enable analysis of dose-response relationships for a single drug, or testing the effects of several different drugs, independently, in freely moving, awake animals. This point should not be ignored as being able to repeatedly deliver drugs and manipulate neuronal activity in an animal without tethers or handling can reduce the critical experimental variables. While battery-free operation allows virtually infinite lifetime of the implanted optofluidic device, reuse of the fluid reservoir is challenging with the current design. We envision that improved designs with refillable or replaceable reservoirs will address this issue to maximize utility of the device. In brief, the ability to manipulate neuronal circuits using wireless optogenetics and pharmacology, together with the possibility of repeated manipulations, represents a significant technological advancement and will allow researchers to ask questions that would have not been possible using existing technologies.

Experimental Section

Design of RF Energy Harvester

The RF harvester (Figure S3, Supporting Information) consists of a stretchable antenna, an impedance matching circuit, and a Villard cascade voltage tripler. Inductors (2.7 and 5 nH; 0.6 mm × 0.3 mm × 0.26 mm) and capacitors (1 pF; 0.6 mm × 0.3 mm × 0.26 mm) are used to match the antenna impedance to the input impedance for maximum power transfer. The signal is rectified and amplified as it passes through the voltage-tripler constructed with Schottky diodes (1PS66SB82, Nexperia; 2 mm × 2.1 mm × 0.9 mm) and capacitors (22 pF; 0.6 mm × 0.3 mm × 0.26 mm). The output DC voltage is stabilized using a decoupling capacitor (0.1 μF; 0.6 mm × 0.3 mm × 0.26 mm) to drive μ-ILEDs or actuate the fluid delivery.

Fabrication of the Battery-Free, Wireless Optofluidic Devices

Construction of the device involves fabrication and integration of an RF harvester and an optofluidic device. The fabrication of an RF harvester starts with spin-casting polymethyl methacrylate (PMMA, 200 nm thick; 495 PMMA A6, Microchem) on a glass substrate followed by curing at 180 °C for 1 h. A PDMS layer (500 μm thick, Sylgard 184, Dow Corning) is prepared by spin-coating and curing on the substrate, and a copper sheet (18 μm thick, DBT-III, Oak-Mitsui) is attached on top. Photolithographic patterning of the copper layer defines the layout of the RF harvester. Attachment of electronic components on the copper layer uses a solder paste (SMD290SNL250T5, Chipquik; curing at 220 °C for 2 min in a reflow oven) for robust bonding. Encapsulation of the entire circuit with another PDMS layer (500 μm thick), followed by releasing by dissolution of the PMMA sacrificial layer in acetone, completes the fabrication. The fabrication protocols for an optofluidic device can be found in refs. [2,38]. The harvester and the optofluidic device are integrated together by connecting the output channels of the harvester to the electrodes of the optofluidic device

using a silver epoxy (H2OE EPO-TEK, Ted Pella Inc.). The two components are sealed and further secured by adding PDMS encapsulation for protection and thermal insulation.

Experimental Subjects

Adult (25–35 g, 8–10 week old) male mice were group-housed, given access to food pellets and water ad libitum, and maintained on a 12:12 h light/dark cycle (lights on at 7:00 AM). All procedures were approved by the Animal Care and Use Committee of Washington University and conformed to US National Institutes of Health (NIH) guidelines.

Implantation of the Device

The optofluidic devices were implanted into the brain of adult mice following a similar method used for our previous soft neural implants.[25] Animals were mounted into a stereotaxic apparatus and anesthetized using isoflurane, while they rested on a heating pad for the duration of the procedure. After securing its head onto the apparatus, the mouse's skull was exposed via a superficial midline incision performed under aseptic conditions. Following the identification of the desired stereotaxic coordinates for the implantation of the device, it was proceeded to drill a small opening for placement of the optofluidic probe. The soft RF harvester was implanted under the skin, caudal to the injection site. Placement of the optofluidic probe into the brain cortex was performed using a stereotaxic holder adapted for these devices, following temporary stiffening of the implant with a biodegradable polymer (poly(lactic-co-glycolic acid); Sigma-Aldrich Inc.). After the implant was secured, the mouse's skin was sutured and the animal was set aside for recovery. The step-by-step process of the surgery can be found in Figure S9 in the Supporting Information. This same method can be referenced in Park et al.[25]

Supplementary Material

Refer to Web version on PubMed Central for supplementary material.

Acknowledgments

K.N.N., S.I.P., and R.Q. contributed equally to this work. This material is based on work supported by Innovative Seed Grant from University of Colorado Boulder (J.-W.J.). J.X. and K.-I.J. acknowledge support from National Science Foundation (CMMI-1405355) and National Research foundation of Korea (NRF-2017M3A7B4049466), respectively. The work was also supported by NIH Director's Transformative Research Award (TR01 NS081707) to R.G. and J.R. and and the McDonnell Center for Cellular and Molecular Neurobiology Postdoctoral Fellowship to A.M.

References

1. Jeong JW, McCall JG, Shin G, Zhang Y, Al-Hasani R, Kim M, Li S, Sim JY, Jang KI, Shi Y, Hong DY, Liu Y, Schmitz GP, Xia L, He Z, Gamble P, Ray WZ, Huang Y, Bruchas MR, Rogers JA. Cell. 2015; 162:662. [PubMed: 26189679]
2. McCall JG, Qazi R, Shin G, Li S, Ikram MH, Jang KI, Liu Y, Al-Hasani R, Bruchas MR, Jeong JW, Rogers JA. Nat Protoc. 2017; 12:219. [PubMed: 28055036]
3. Yizhar O, Fenno LE, Davidson TJ, Mogri M, Deisseroth K. Neuron. 2011; 71:9. [PubMed: 21745635]
4. Kramer RH, Mourot A, Adesnik H. Nat Neurosci. 2013; 16:816. [PubMed: 23799474]
5. Tye KM, Deisseroth K. Nat Rev Neurosci. 2012; 13:251. [PubMed: 22430017]

6. Gradinaru V, Mogri M, Thompson KR, Henderson JM, Deisseroth K. Science. 2009; 324:354. [PubMed: 19299587]
7. Yamamoto K, Tanei Z, Hashimoto T, Wakabayashi T, Okuno H, Naka Y, Yizhar O, Fenno LE, Fukayama M, Bito H, Cirrito JR, Holtzman DM, Deisseroth K, Iwatsubo T. Cell Rep. 2015; 11:859. [PubMed: 25937280]
8. Zalocusky KA, Ramakrishnan C, Lerner TN, Davidson TJ, Knutson B, Deisseroth K. Nature. 2016; 531:642. [PubMed: 27007845]
9. Busskamp V, Picaud S, Sahel JA, Roska B. Gene Ther. 2012; 19:169. [PubMed: 21993174]
10. Bruegmann T, Malan D, Hesse M, Beiert T, Fuegemann CJ, Fleischmann BK, Sasse P. Nat Methods. 2010; 7:897. [PubMed: 20881965]
11. Kravitz AV, Tye LD, Kreitzer AC. Nat Neurosci. 2012; 15:816. [PubMed: 22544310]
12. Felix-Ortiz AC, Burgos-Robles A, Bhagat ND, Leppla CA, Tye KM. Neuroscience. 2016; 321:197. [PubMed: 26204817]
13. Nguyen JK, Park DJ, Skousen JL, Hess-Dunning AE, Tyler DJ, Rowan SJ, Weder C, Capadona JR. J Neural Eng. 2014; 11:056014. [PubMed: 25125443]
14. Cai DJ, Aharoni D, Shuman T, Shobe J, Biane J, Song W, Wei B, Veshkini M, La-Vu M, Lou J, Flores SE, Kim I, Sano Y, Zhou M, Baumgaertel K, Lavi A, Kamata M, Tuszynski M, Mayford M, Golshani P, Silva AJ. Nature. 2016; 534:115. [PubMed: 27251287]
15. Copits BA, Pullen MY, Gereau RW IV. Pain. 2016; 157:2424. [PubMed: 27340912]
16. Kim T, McCall JG, Jung YH, Huang X, Siuda ER, Li Y, Song J, Song YM, Pao HA, Kim RH, Lu C, Lee SD, Song IS, Shin G, Al-Hasani R, Kim S, Tan MP, Huang Y, Omenetto FG, Rogers JA, Bruchas MR. Science. 2013; 340:211. [PubMed: 23580530]
17. Canales A, Jia X, Froriep UP, Koppes RA, Tringides CM, Selvidge J, Lu C, Hou C, Wei L, Fink Y, Anikeeva P. Nat Biotechnol. 2015; 33:277. [PubMed: 25599177]
18. Minev IR, Musienko P, Hirsch A, Barraud Q, Wenger N, Moraud EM, Gandar J, Capogrosso M, Milekovic T, Asboth L, Torres RF, Vachicouras N, Liu Q, Pavlova N, Duis S, Larmagnac A, Vörös J, Micera S, Suo Z, Courtine G, Lacour SP. Science. 2015; 347:159. [PubMed: 25574019]
19. Kim BJ, Kuo JTW, Hara SA, Lee CD, Yu L, Gutierrez CA, Hoang TQ, Pikov V, Meng E. J Neural Eng. 2013; 10:045002. [PubMed: 23723130]
20. Luan L, Wei X, Zhao Z, Siegel JJ, Potnis O, Tuppen CA, Lin S, Kazmi S, Fowler RA, Holloway S, Dunn AK, Chitwood RA, Xie C. Sci Adv. 2017; 3:e1601966. [PubMed: 28246640]
21. Sim JY, Haney MP, Park SI, McCall JG, Jeong JW. Lab Chip. 2017; 17:1406. [PubMed: 28349140]
22. Jeong JW, Shin G, Park SI, Yu KJ, Xu L, Rogers JA. Neuron. 2015; 86:175. [PubMed: 25856493]
23. Hashimoto M, Hata A, Miyata T, Hirase H. Neurophotonics. 2014; 1:011002. [PubMed: 26157963]
24. Park SI, Brenner DS, Shin G, Morgan CD, Copits BA, Chung HU, Pullen MY, Noh KN, Davidson S, Oh SJ, Yoon J, Jang K-I, Samineni VK, Norman M, Grajales-Reyes JG, Vogt SK, Sundaram SS, Wilson KM, Ha JS, Xu R, Pan T, Kim T, Huang Y, Montana MC, Golden JP, Bruchas MR, Gereau RW IV, Rogers JA. Nat Biotechnol. 2015; 33:1280. [PubMed: 26551059]
25. Park SI, Shin G, McCall JG, Al-Hasani R, Norris A, Xia L, Brenner DS, Noh KN, Bang SY, Bhatti DL, Jang KI, Kang SK, Mickle AD, Dussor G, Price TJ, Gereau RW, Bruchas MR, Rogers JA. Proc Natl Acad Sci USA. 2016; 113:E8169. [PubMed: 27911798]
26. Montgomery KL, Yeh AJ, Ho JS, Tsao V, Mohan Iyer S, Grosenick L, Ferenczi EA, Tanabe Y, Deisseroth K, Delp SL, Poon ASY. Nat Methods. 2015; 12:969. [PubMed: 26280330]
27. Metz S, Holzer R, Renaud P. Lab Chip. 2001; 1:29. [PubMed: 15100886]
28. Takeuchi S, Ziegler D, Yoshida Y, Mabuchi K, Suzuki T. Lab Chip. 2005; 5:519. [PubMed: 15856088]
29. Ziegler D, Suzuki T, Takeuchi S. J Microelectromech Syst. 2006; 15:1477.
30. Metz S, Bertsch A, Bertrand D, Renaud P. Biosens Bioelectron. 2004; 19:1309. [PubMed: 15046764]
31. McCall JG, Jeong JW. Curr Opin Pharmacol. 2017; 36:78. [PubMed: 28892801]
32. Harrington, RF. Time-Harmonic, Electromagnetic Fields. Wiley-IEEE; New York, NY: 2001.

33. Wu X, Zhang Y, Takle K, Bilsel O, Li Z, Lee H, Zhang Z, Li D, Fan W, Duan C, Chan EM, Lois C, Xiang Y, Han G. ACS Nano. 2016; 10:1060. [PubMed: 26736013]
34. Zhang Y, Huang L, Li Z, Ma G, Zhou Y, Han G. ACS Nano. 2016; 10:3881. [PubMed: 27077481]
35. Federal Communications Commission. Code of Federal Regulations, Title 47. Vol. 15. Washington D.C., USA: 2014. p. 825
36. Carreker RP, Hibbard WR. Acta Metall. 1953; 1:654.
37. Shin G, Gomez AM, Al-Hasani R, Jeong YR, Kim J, Xie Z, Banks A, Lee SM, Han SY, Yoo CJ, Lee J-L, Lee SH, Kurniawan J, Tureb J, Guo Z, Yoon J, Park S-I, Bang SY, Nam Y, Walicki MC, Samineni VK, Mickle AD, Lee K, Heo SY, McCall JG, Pan T, Wang L, Feng X, Kim T, Kim JK, Li Y, Huang Y, Gereau RW IV, Ha JS, Bruchas MR, Rogers JA. Neuron. 2017; 93:509. [PubMed: 28132830]
38. McCall JG, Kim T, Shin G, Huang X, Jung YH, Al-Hasani R, Omenetto FG, Bruchas MR, Rogers JA. Nat Protoc. 2013; 8:2413. [PubMed: 24202555]

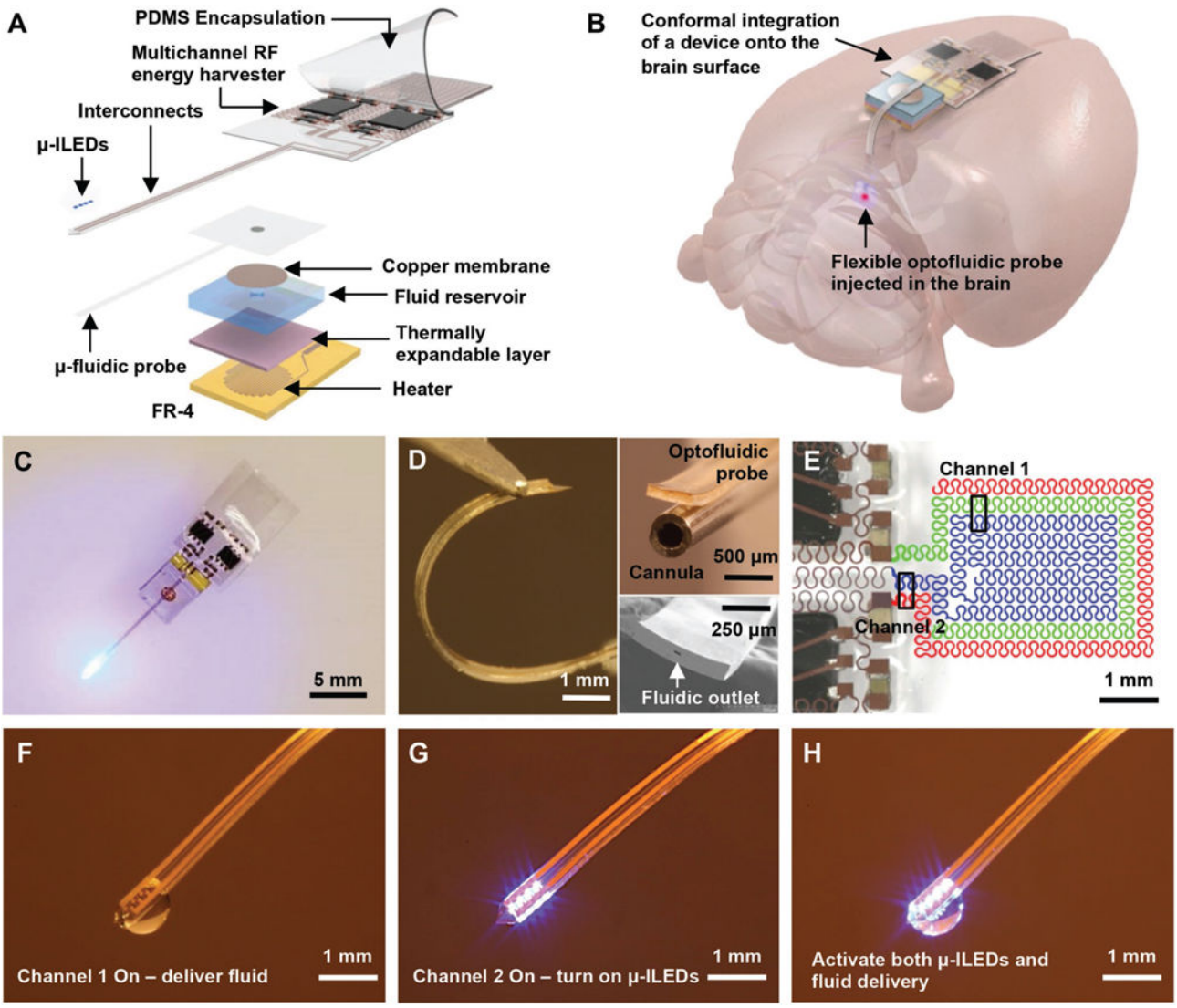

Figure 1.

Design and operational features of fully implantable, battery-free, wireless optofluidic neural probe systems. A) Exploded view schematic illustration of a soft optofluidic system. B) Conceptual diagram illustrating conformal integration of the wireless optofluidic system and probe implantation in a rodent brain. The device can be oriented differently, depending on the location of the target brain region. C) Optical image of an optofluidic device to illustrate its fully wireless capabilities. D) Optical image of an optofluidic probe that illustrates the flexible mechanics (left). Optical image comparing sizes of the optofluidic probe and the traditional metal cannula (right top) and scanning electron image of the fluidic outlet at the tip of probe (right bottom). E) False-colored optical image of a stretchable RF antenna with two capacitive coupling channels. Optical images showing versatile controls of the optofluidic device for F) fluid delivery, G) μ-ILEDs, and H) simultaneous activation of μ-ILEDs and fluid delivery via a two-channel wireless energy harvester.

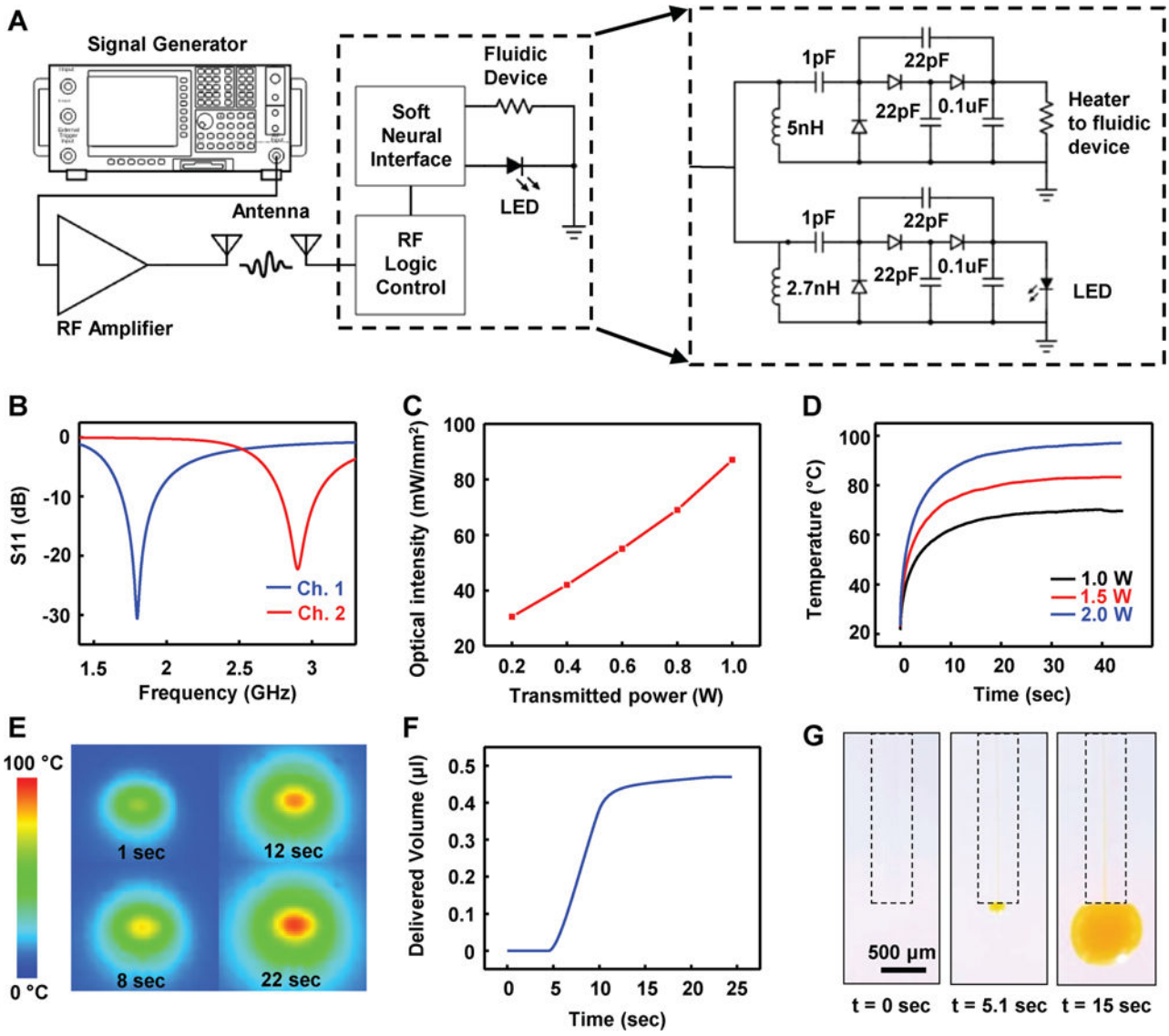

Figure 2.

Electrical, optical, and thermal characteristics of battery-free, wireless optofluidic systems with two-channel stretchable antennas. A) Schematic diagram showing the overall setup for operation of a two-channel wireless optofluidic system (left) and its detailed circuit diagram (right). B) Scattering parameter S_{11} of the two-channel antenna (channel 1, blue; channel 2, red). C) Optical intensity of μ-ILEDs as a function of RF power transmitted from 10 cm away. D) Heater temperature variation with different RF power transmissions. E) Time sequence of IR images of the heater showing the temperature increase. F) Delivered fluid volume as a function of time when 2 W of the RF power is transmitted. G) Sequential images of fluid delivery through a microfluidic probe.

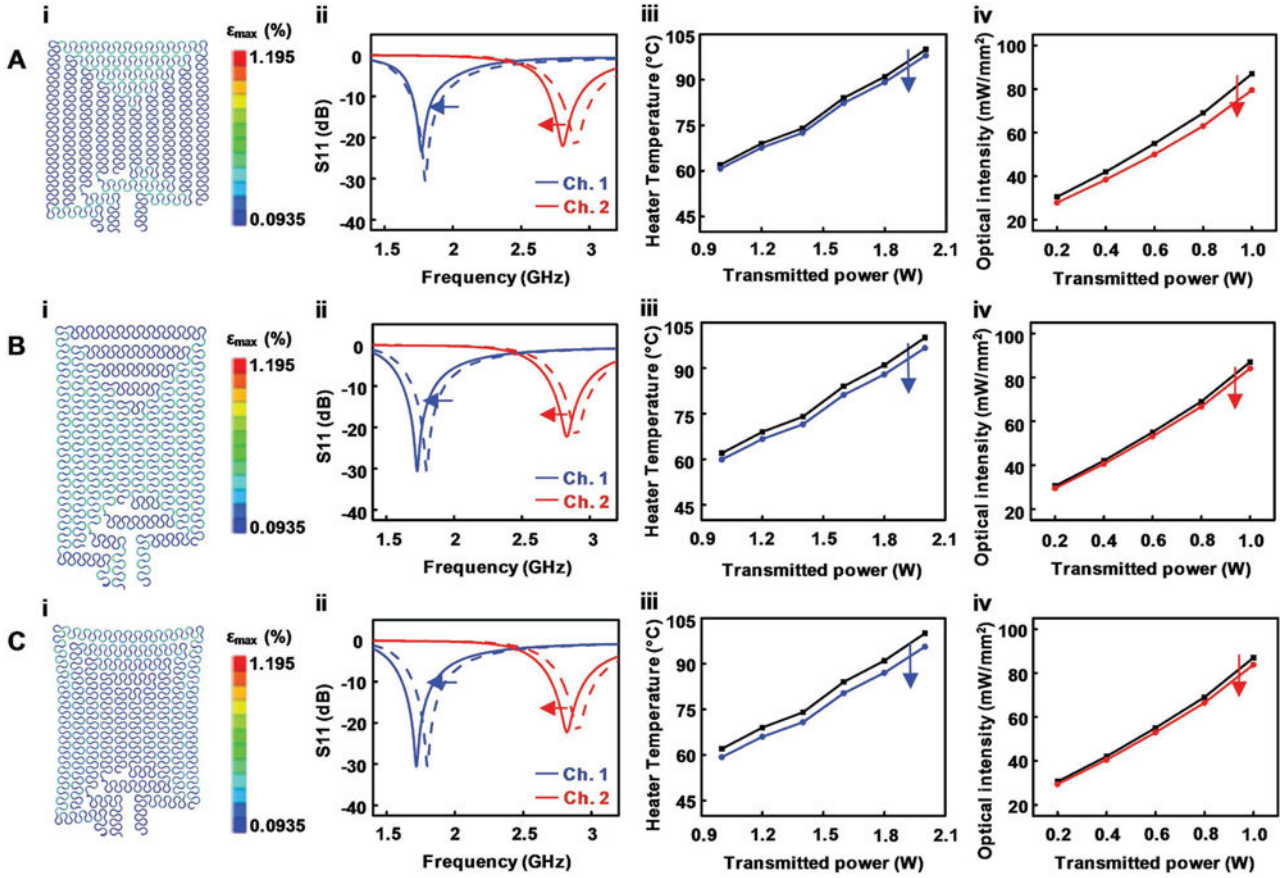

Figure 3.

Response of a wireless optofluidic system under mechanical deformation of its stretchable antenna. Functional characteristic shifts of an optofluidic system under A) 20% uniaxial horizontal stretching, B) 20% uniaxial vertical stretching, and C) 20% biaxial diagonal stretching. i) FEA simulation showing the resulting strain in the stretchable antenna structure under deformation. ii) S_{11} shift in each channel. iii) Shift in heater temperature at 25 s. iv) Shift in the optical intensity of μ-ILEDs.

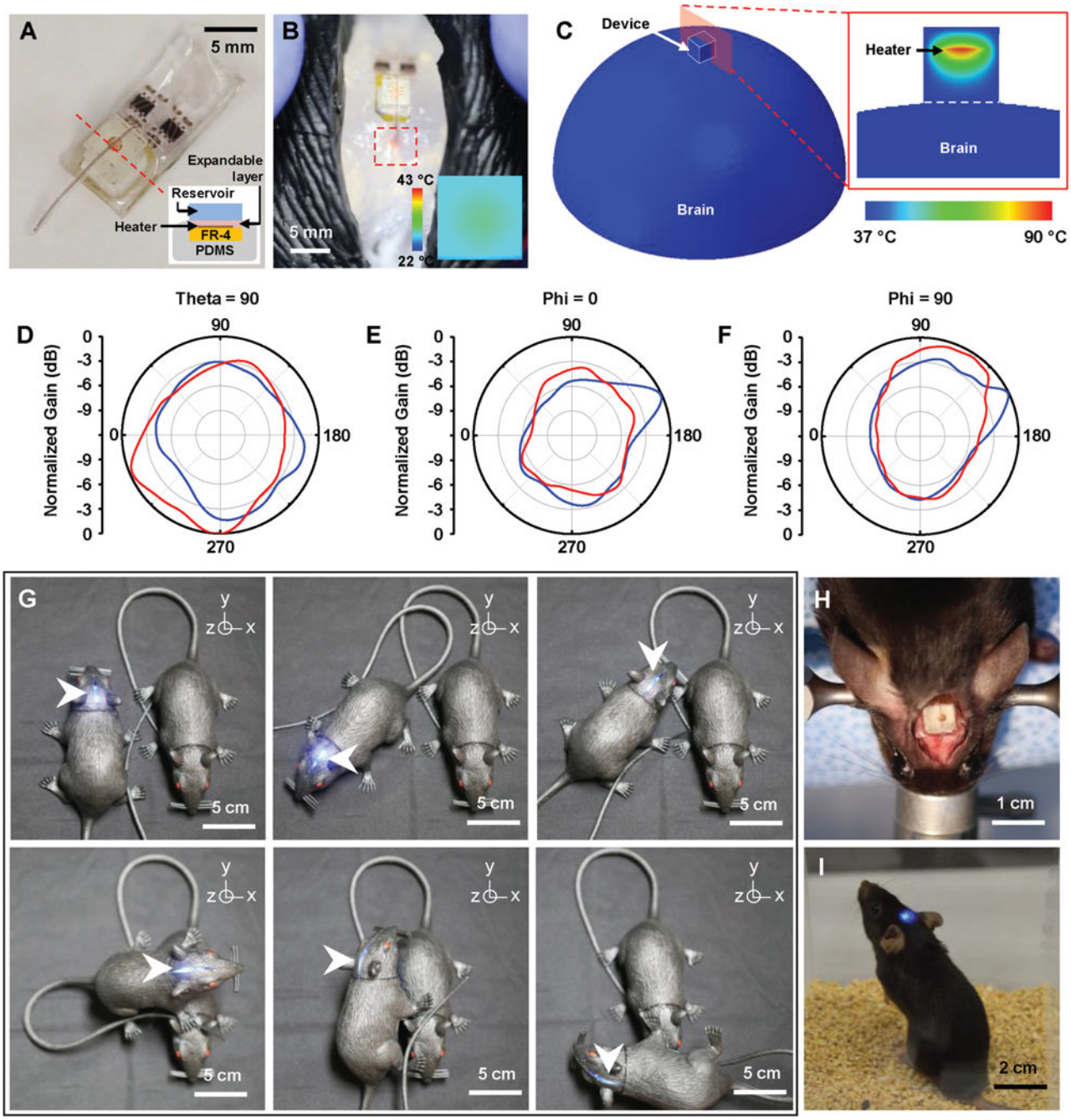

Figure 4.

Feasibility study of fully implantable, battery-free, wireless optofluidic systems for operation in freely moving animals. A) Optical image of a wireless optofluidic device encapsulated with 2 mm thick PDMS for thermally safe operation of the heater on brain tissue. The inset shows the cross-sectional image of the device, defined by the red dotted line. B) Wireless delivery of red dye into the phantom brain (0.6% agarose gel) in the rat model. The red dotted box indicates the infused dye. IR image in the inset shows surface temperature of the heater's PDMS encapsulant (≈30 °C) in ambient environment at room temperature when the heater temperature reaches ≈100 °C during fluid delivery, verifying

rapid heat dissipation through the PDMS encapsulant. C) FEA modeling of temperature distribution at the surface of the 3D model simulating the device operated on the brain surface (left) and that at the cross-section cut by the red plane (right). D–F) Normalized angular radiation pattern of two-channel antennas in optofluidic systems. Cross-sectional view at D) $\theta = 90°$, where polar angle θ is the angle measured from the zenith direction of the antenna plane, E) $\varphi = 0°$, where azimuthal angle φ is the angle measured from the orthogonal projection onto the antenna plane from the direction toward the antenna input, and F) $\varphi = 90°$. G) Pictures of a model rat implanted with a wireless optofluidic system, demonstrating wireless operation at various angles. H) Optical image showing full implantation of an optofluidic device into a mouse's head. I) Optical image of a freely behaving mouse with an optofluidic device implanted under the skin, on the skull.